ACS APPLIED BIO MATERIALS

www.acsabm.org

Article

Single-Cell Analysis of Unidirectional Migration of Glioblastoma Cells Using a Fiber-Based Scaffold

Norichika Hashimoto,* Ryuhei Kitai, Satoshi Fujita,* Takahiro Yamauchi, Makoto Isozaki, and Ken-Ichiro Kikuta

Cite This: *ACS Appl. Bio Mater.* 2023, 6, 765−773

Read Online

ACCESS | Metrics & More | Article Recommendations | Supporting Information

ABSTRACT: Glioblastoma (GBM) is a malignant incurable brain tumor in which immature neoplastic cells infiltrate brain tissue by spreading along nerve fibers. The aim of the study was to compare the migration abilities of glioma cells with those of other cancer cells and elucidate the migratory profiles underlying the differential migration of glioma cells using a fiber-based quantitative migration assay. Here, wound healing and transwell assays were used to assess cell mobility in four cell lines: U87-MG glioblastoma cells, MDA-MB-231 breast cancer cells, HCT116 colorectal cancer cells, and MKN45 gastric cancer cells. We also assessed cell mobility using a fiber model that mimics nerve fibers. Time-lapse video microscopy was used to observe cell migration and morphology. The cytoskeleton arrangement was assessed in the fiber model and compared with that in the conventional cell culture model. The conventional evaluation of cell migration ability revealed that the migration ability of breast cancer and glioblastoma cell lines was higher than that of colon cancer and gastric cancer cell lines. The fiber model confirmed that the glioblastoma cell line had a significantly higher migration ability than other cell lines. Tubulin levels were significantly higher in the glioblastoma cells than in other cell lines. In conclusion, the developed fiber-based culture model revealed the specific migratory profile of GBM cells during invasion.

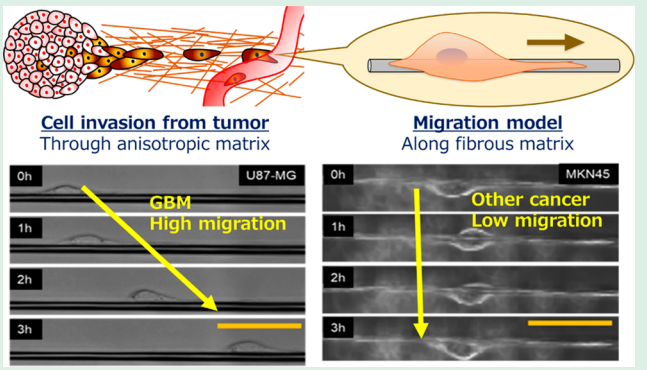

KEYWORDS: *glioblastoma, migration, invasion, electrospun fiber, single-cell analysis*

1. INTRODUCTION

Glioblastoma (GBM) has an extremely poor prognosis despite multidisciplinary treatments such as surgery, chemotherapy, and radiation therapy.[1−3] GBM malignancy is characterized by its highly proliferative,[4] angiogenic,[5] and invasive[6] properties. The gold standard of surgical treatment is maximum safety resection, which means complete resection with remarkable contrast enhancement but low neurological deterioration.[7] The glioma cells in the enhanced area invade the adjacent brain, especially in the contralateral hemisphere and along nerve fibers;[8] therefore, GBM inevitably recurs at the invasion site.[9]

The invasion mechanism of unresectable gliomas has been extensively studied by neurooncologists. In the 1930s, neuropathologists examined the sectioned brains of 100 patients with glioma and reported that tumor cells migrated along existing brain structures in formations called secondary structures.[10,11] GBM infiltrates along nerve fibers and blood vessels; however, metastatic lesions are rarely seen at the initial stage. Metastatic lesions are observed in recurrence and terminal images on the contralateral side of cerebral hemisphere with lesions; they are observed via white matter tracts of the corpus callosum and along optic radiations and fornix and anterior commissure, appearing visually as the shadow of a butterfly.[12] Recently, investigators have focused on invasion pathways, including the brain parenchyma microenvironment,[13] blood vessels,[14] the subarachnoid space,[15] and nerve fibers in the white matter.[8] Research on glioma invasion has been widening to include morphological changes, epithelial and mesenchymal transformation,[16] chemical interactions such as chemokines,[17] relationships with the extracellular matrix,[18] and inhibitory agents.[19]

Tumor invasion is strongly related to cell migration; thus, simple and effective methods to assess glioma migration are highly desired. To clarify the biological aspects of migration, various experimental assays are used, including wound healing[20] and Boyden chamber assays.[21] The wound healing assay is an easy way to assess collective cell migration.[22] The

Received: November 14, 2022
Accepted: February 1, 2023
Published: February 9, 2023

https://doi.org/10.1021/acsabm.2c00958
ACS Appl. Bio Mater. 2023, 6, 765−773

Boyden chamber assay is used to elucidate the migration of cells through a porous membrane.[23] However, neither method is appropriate for characterizing migration at the single-cell level. Additionally, conventional methods to analyze cell migration are not suited to investigate unidirectional migration along a fibrous microenvironment.

In our previous study, we analyzed cell migration activity on a sheet of aligned fibers with different densities, mimicking brain fibrous matrix structures, and revealed that the velocity and directionality of cells were affected by the density of fibers.[24] Cells cultured on sparser fibers with fewer adhesion points exhibited low migratory activity. By further reducing the fiber density and culturing cells under conditions in which a single cell adheres to only one fiber, cell migration would be expected to be limited to movement in only one axis, forward and backward, and could be analyzed quantitatively. Here, we developed a fiber-based assay using a geometrically controlled scaffold of single-bridged aligned fibers that act as a rail mimicking the fibrous microenvironment of the brain. This permits us to investigate GBM invasion at the single-cell level, observe dynamic changes in cell migration under conditions similar to those in the brain, and quantitate the mobility of cells in the GBM compared with that of other malignant tumor cells at the single-cell level. This novel method will help elucidate the mechanism of cell migration and lead to the development of therapeutic agents aimed at inhibiting tumor cell migration.

2. MATERIALS AND METHODS

2.1. Cell Culture. U87-MG human glioma cells, MDA-MB-231 human breast cancer cells, and HCT116 human colon cancer cells were obtained from the American Type Culture Collection (ATCC). MKN45 human gastric cancer cells were obtained from the Riken Cell Bank (Tsukuba, Japan). Cells were maintained in Dulbecco's modified Eagle's medium (DMEM; #D5796, Sigma-Aldrich Japan, Tokyo, Japan), supplemented with 10% fetal bovine serum (FBS; #F-0500-A, Atlas Biologicals Inc., Fort Collins, CO, USA), 1% glutamine, and 1% penicillin/streptomycin (#06168-34, Nacalai Tesque, Kyoto, Japan), and cultured under 5% CO_2 at 37 °C.

2.2. Wound Healing Assay. Each cell line (5.0×10^5 cells) was seeded into 35 mm dishes (#3000−035, Iwaki, Tokyo, Japan) and cultured overnight to reach confluence in DMEM supplemented with 10% FBS under humidified 5% CO_2 at 37 °C. The cell monolayer was scratched with a sterile 200 μL pipet tip to produce a wound approximately 800 μm wide. Then, the cells were washed once with culture medium and incubated in normal culture conditions. The scratched areas were observed using a microscope (FV10i-w, Olympus, Tokyo, Japan) after 0, 4, 8, and 12 h. The wound areas were measured from binarized optical microscopic images (1×1 mm area for each measurement) using ImageJ software (ver. 1.48, NIH, USA). The experiments were performed using five replicates.

2.3. Transwell Migration Assay. Cell migration was evaluated using CytoSelect 24-Well Cell Migration Assay Kit, which contains polycarbonate membrane inserts (8 μm pore size) (#CBA-100-C, Cell Biolabs, San Diego, CA, USA). Cells were suspended in serum-free DMEM and seeded at 1×10^4 cells/well in the upper chamber. After 1 h, 500 μL of DMEM containing 10% FBS was added to the lower well, and the cells were cultured for 24 h. The number of cells that passed through the polycarbonate membrane was measured by colorimetry (560 nm absorbance) using a plate reader (SpectraMax M5; Molecular Devices, CA, USA). The experiments were performed five times.

2.4. Fabrication of the Fiber-Based Scaffold. Sparse polystyrene fine fibers were electrospun using a commercial electrospinning setup (NANON-01A, MECC, Fukuoka, Japan) consisting of a power supply, syringe, syringe pump, needle, and a grounded rotary disk-shaped collector, as described in our previous study.[24] Briefly, using an applied high voltage, polystyrene/tetrahydrofuran solution (20% w/v) was injected out of the needle at a constant flow rate toward the grounded rotating collector to obtain fibers aligned in one direction onto the handmade acrylic jig. The jig was cut out with a laser processing machine and fitted on a 35 mm glass-bottom dish (#D11130H, Matsunami Glass Ind., Ltd., Osaka, Japan). The electrospinning conditions were as follows: flow rate, 0.5 mL/h; rotation speed, 1500 rpm; applied electric field, 2.5 kV/cm; and spinning time, 10 s. The short-term electrospinning provided independent single fibers. To improve the fiber surface hydrophilicity and to sterilize the fibers, the substrate was washed with 70% ethanol and subjected to oxygen plasma treatment (40 kHz, 100 W, 30 s, 0.1 MPa) using a plasma reactor (Diener Electronics, Ebhausen, Germany).

2.5. Scanning Electron Microscopy (SEM). Specimens were sputter-coated with Pt/Pd (120 s, 15 mA, 6 Pa) prior to SEM (JSM-6390, JEOL, Tokyo, Japan) analysis at an applied voltage of 15 kV. The fiber diameters were measured from SEM images (1280×960 pixels; nine different fields were randomly selected) using ImageJ (ver. 1.52e).

2.6. Fiber Migration Assay. Cells were seeded onto the fibers at 1.0×10^3 cells/dish. After preculture for 2 h, single cells that adhered to the fiber were tracked by imaging every 10 min for 3 h using a time-lapse microscope (FV10i-w, Olympus). The total migration distance was measured using ImageJ. Five cells were analyzed for each measurement.

Directionality was defined as the distance between the start and end locations in the observation time (L_{total}) divided by the net distances of the cell trajectories at each time point (L_i), as shown in eq 1.

$$\text{directionality} = \frac{L_{total}}{\sum L_i} \tag{1}$$

A directionality ratio = 1 indicated that the cells migrated in one direction. A smaller direction ratio was associated with lower directivity or migration activity.

2.7. Immunochemistry. U87-MG, MDA-MB-231, HCT116, and MKN45 cell lines were used to evaluate actin and tubulin production during migration. Cells were seeded at 1×10^5 cell/mL on a flat dish and cultured in DMEM containing 10% FBS in a single-cell suspension at 37 °C and 5% CO_2 for 24 h. Another group of cells was also seeded uniformly on a fiber scaffold running parallel to a glass slide fitted into a four-well rectangular dish (#167063, Thermo Fisher Scientific K.K., Tokyo, Japan). After 24 h, the cultures were washed three times with PBS. Subsequently, 1 μL of protease inhibitor (#P8215−1M, Sigma) was added to 100 μL of RIPA buffer (#16488−34, Nacalai Tesque) and coated onto the cells. Then, the cells were collected and exposed to ambient air on ice for 30 min before centrifuging at 4 °C and 400g for 20 min. The supernatant was collected, and 5 μg of supernatant protein per lane was electrophoresed on a 10−20% gel (E-R1020L ePAGEL #2331740, ATTO, Tokyo, Japan) at 20 mA for 80 min. The bands were transferred to a semidry PVDF membrane. The membranes were blocked with EzChemi AE-1475 (#2332615, ATTO) and labeled with the following primary antibodies (1:1000): mouse anti-α-tubulin (B-7, #sc-5286, Santa Cruz Biotechnology, Inc., Santa Cruz, CA, USA),[25] mouse anti-β-actin (8H10D10, #3700, Cell Signaling Technology, Danvers, MA, USA),[26] and mouse antiglyceraldehyde-3-phosphate dehydrogenase (GAPDH; 6C5; #MAB374, Merck Millipore, Tokyo, Japan).[27] After washing, the membranes were incubated with 1:1000 diluted-peroxidase-labeled secondary antibody (HRP AffinPure Goat Anti-Mouse IgG, #115−035−072, Jackson ImmunoResearch Inc., West Grove, PA, USA).[28] The validation of antibody specificity was omitted, but only those that have been fully characterized were selected in this study. Method specificity was confirmed by omitting primary antibodies in the reaction sequence, which served to confirm the specificity of secondary antibodies. The bands were visualized using a chemiluminescence detector (LAS4000 mini, GE Healthcare

https://doi.org/10.1021/acsabm.2c00958
ACS Appl. Bio Mater. 2023, 6, 765−773

Life Sciences, Tokyo, Japan). Image analysis was performed using ImageQuant TL analysis software. The experiments were performed five times.

2.8. Time-Lapse Observation of Cytoskeletal Proteins. Dynamic observation of cytoskeleton localization in living cells was performed using the Cell Light Reagent Bacman2.0 Tubulin-GFP and Actin-RFP (#C10583 and C10613, Thermo Fisher) according to the manufacturer's guidelines.[29] Fluorescently labeled cells were seeded onto fibers at 1.0×10^3 cells/mL and tracked for 3 h using a time-lapse microscope (FV10i-w, Olympus).

2.9. Statistical Methods. The experimental values are expressed as mean values with standard deviations of independent n experiments. To determine n, we confirmed the standard deviation and the normality of distribution of the experimental data in a preliminary study. When the true difference in the groups was twice the standard deviation, we needed to study $n = 4$ to be able to reject the null hypothesis that the population means of the experimental and control groups were equal with a power = 0.8. The Type I error probability associated with this test of the null hypothesis was 0.05. Considering the possibility of outliers, the actual measurement was performed with $n = 5$. The normality of the distribution was confirmed using the Kolmogorov–Smirnov test, and then, the homoscedasticity was examined using the Bartlett test. Comparisons between groups were made using ANOVA if homoscedasticity was assumed; otherwise, the Kruskal–Wallis test (GraphPad Software, La Jolla, CA, USA) was used. $p < 0.05$ was considered statistically significant. To minimize subjective bias in the research, the order of the samples was randomized, and the experimenter was blinded to the experimental protocol while performing the experiments and the statistical calculations.

3. RESULTS

3.1. U87-MG and MDA-MB-231 Cells Showed Higher Migration in the Wound Healing Assay. Four cell lines—U87-MG glioblastoma cells, MDA-MB-231 breast cancer cells, HCT116 colorectal cancer cells, and MKN45 gastric cancer cells—were used to evaluate cancer cell migration using the conventional wound healing assay. To minimize the effect of cell proliferation, cell migration was evaluated on a flat plate within 12 h. HCT116 and MKN45 cells maintained their cobblestone-like shape and lower wound healing activity, whereas U87-MG and MDA-MB-231 cells showed higher migration activity (Figure 1a). In particular, some of the U87-MG cells showed spindle and elongated shapes and escaped from the original colony and actively migrated at 12 h. The percentage of the wound area covered with U87-MG, MDA-MB-231, HCT116, and MKN45 cells after 12 h was 49.4 ± 5.3, 52.9 ± 9.6, 22.6 ± 4.9, and 16.3 ± 3.3%, respectively (Figure 1b). The percentage of the cell-filled wound area in the U87-MG and MDA-MB-231 cell lines was significantly higher than that in the MKN45 cell line at 12 h.

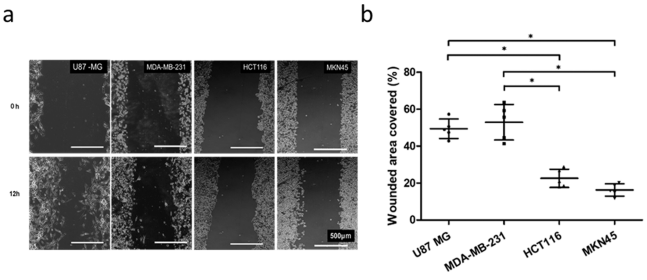

Figure 1. U87-MG and MDA-MB-231 cells showed higher migration activity in the wound healing assay. (a) Phase contrast images at 0 and 12 h. Scale bar = 500 μm. (b) Percentage of covered area at 12 h. Values represent means ± SD $n = 5$; *$p < 0.05$.

3.2. U87-MG and MDA-MB-231 Cells Also Showed Higher Invasion Activity in the Transwell Migration Assay. The Boyden chamber assay, which is also called the transwell membrane assay, is a classical method for evaluating cell invasion. In this method, cells are cultured on one side of a porous membrane, and the number of cells passing through the membrane is counted. Here, cell invasion through a membrane with 8 μm pores was evaluated after 24 h to evaluate invasive migration activity. Microscopic images showed that U87-MG and MDA-MB-231 cells had higher invading activity than that of HCT116 and MKN56 cells (Figure 2a). To quantify the number of invading cells, the absorbance of the stained cells was measured using a plate reader. The absorbance of U87-MG, MDA-MB231, HCT116, and MKN45 cells was 1.01 ± 0.12, 0.90 ± 0.22, 0.61 ± 0.25, and 0.52 ± 0.04, respectively (Figure 2b). U87-MG and MDA-MB-231 cells showed significantly higher absorbance than that of MKN45 cells. These results were consistent with the wound-healing assay results.

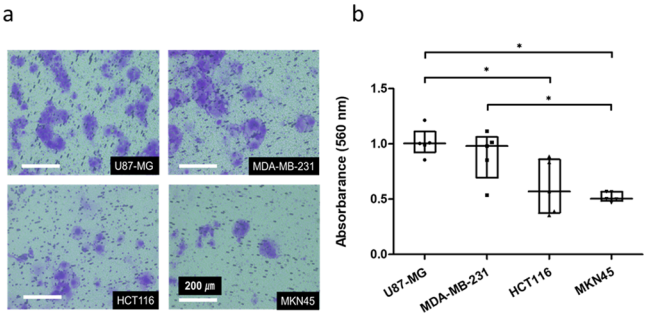

Figure 2. U87-MG and MDA-MB-231 cells showed higher invasion activity in the transwell migration assay. (a) Phase contrast images of cells that migrated through the membrane. The cells were stained with reagents from CytoSelect 24-Well Cell Migration Assay kit. Scale bar = 200 μm. (b) Colorimetric measurement (560 nm absorbance) of migrated cells. Values represent medians and IQR. $n = 5$; *$p < 0.05$.

3.3. Fabrication of a Device for a Fiber-Based Single-Cell Migration Assay. A fiber-based assay was performed to evaluate mesenchymal migration. To track the migration of single cells, a fiber-based scaffold was fabricated by collecting electrospun fibers oriented in the same direction onto a glass coverslip. The fabricated fibers had a smooth surface, and their average diameter was 5.38 ± 1.37 μm ($n = 39$) as determined by SEM observation (Figures 3 and S1).

3.4. U87-MG Cells Showed the Fastest Migration in the Fiber-Based Single-Cell Migration Assay. To investigate the cell invasive activity at a single-cell level, cell migration along with a fibrous structure was investigated using the fiber-based migration assay. The four cell lines were thoroughly dispersed into single cells by trypsin treatment. The cells were then seeded on the fiber scaffold with a pipet and tracked with time-lapse microscopy. As shown in Figure 4a and Supplementary Movies S1, S2, S3, and S4, U87-MG cells exhibited faster migration on the fibers than that of the other cell lines. These cells also maintained an elongated shape during migration. The total migration distance of U87-MG, MDA-MB-231, HCT116, and MKN45 cells over 3 h was 246 ± 129, 84 ± 34, 55 ± 12, and 23 ± 14 μm, respectively (Figure 4b).

https://doi.org/10.1021/acsabm.2c00958
ACS Appl. Bio Mater. 2023, 6, 765−773

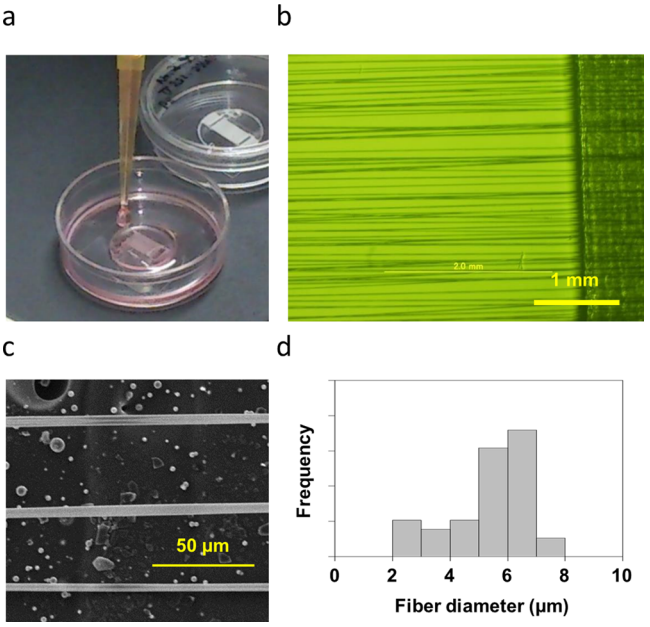

Figure 3. Fabrication of the fiber-based scaffold. (a) Experimental setup. (b) Macroscopic image of fabricated fiber scaffold. (c) SEM image of electrospun fibers. (d) Distribution of fiber diameter.

When the tumor cells were cultured on the fibers in single-cell suspensions, some of the cells migrated in one direction, while others moved back and forth. Thus, we observed and evaluated the direction of tumor cell migration. The directionality of U87-MG, MDA-MB-231, HCT116, and MKN45 cells was 0.88 ± 0.15, 0.31 ± 0.20, 0.46 ± 0.15, and 0.46 ± 0.17, respectively (Figure 4c). U87-MG cells had a directionality close to 1, indicating that their migration on the fiber was unidirectional. Conversely, other cell lines exhibited random migratory movements along the fiber.

3.5. Tubulin Expression Was Higher in U87-MG Cells but the Culture Scaffold Had No Effect on Tubulin or Actin Expression. We investigated whether the expression levels of cytoskeletal tubulin and actin differed depending on the cell line and the culture scaffold. The cells were cultured in a conventional flat dish or on the fiber scaffold. After 24 h, most cells were maintained in a single-cell state in both culture conditions. After normalizing to GAPDH expression, we found that cytoskeletal tubulin expression was markedly higher in U87-MG cells (Figure 5a,b). The ratios of tubulin and GAPDH expression in cells cultured in conventional dishes were 0.97 ± 0.05, 0.28 ± 0.23, 0.33 ± 0.28, and 0.22 ± 0.14 for U87-MG, MDA-MB-231, MKN45, and HCT116 cells, respectively. The tubulin:GAPDH ratio of cells cultured on the fiber scaffold was 0.87 ± 0.45, 0.20 ± 0.09, 0.25 ± 0.20, and 0.20 ± 0.18 for U87-MG, MDA-MB-231, HCT116, and MKN45 cells, respectively. No significant difference was observed in the tubulin:GAPDH ratio between cells cultured on conventional and fiber scaffolds. Statistical analysis is shown in Table S1.

The actin:GAPDH expression ratio was similar in all of the cell types cultured on both scaffolds (Figures 5a,c and S2). We observed that the actin:GAPDH ratios of cells cultured in conventional dishes were 0.88 ± 0.30, 1.37 ± 0.69, 1.02 ± 0.49, and 1.18 ± 0.64 for the U87-MG, MDA-MB-231, HCT116, and MKN45 cells, respectively. The ratios for cells cultured on the fiber scaffold were 0.77 ± 0.34, 1.48 ± 0.66, 0.85 ± 0.41, and 0.92 ± 0.17 for U87-MG, MDA-MB-231, HCT116, and MKN45 cells, respectively. No significant differences were observed among the groups (Table S2).

3.6. Tubulin Extended along Cells on the Fiber Scaffold. To investigate the localization of tubulin in the cells, we stained cytoskeletal proteins in U87-MG cells cultured on a fiber scaffold to visualize the direction of the microtubular extension from the central body and the direction of cell movement (Figure 5d). Tubulin was observed to extend in the same direction as the cells elongated. Actin staining showed dynamic aggregation at both ends that entangled with the fiber. The observed cells were multinucleated, a characteristic of the glioblastoma cell line, and there were no multiple adhered cells. Furthermore, the cells were not two dividing cells, because dividing cells usually do not migrate.

4. DISCUSSION

Here, we focused on tumor cell migration along fibrous structures in brain metastasis. Four tumor cell lines, including glioma cells, were selected and investigated with cell lines of highly malignant cancers that commonly show brain metastases.[30] Wound healing and transwell assays revealed that U87-MG GBM cells and MDA-MB-231 breast cancer cells showed higher migration than that of HCT116 colorectal cancer cells and MKN45 gastric cancer cells. Although the migratory activity of U87-MG and MDA-MB-231 cells did not show significant differences in conventional assays, our fiber-based assay revealed that the migratory activity of U87-MG cells was higher than that of MDA-MB-231 cells. Time-lapse images revealed the movement direction, velocity, and cell shape. In previous reports, individual GBM cells radiated outward from the tumor core along fibrous structures,[31,32] which is unique compared to other solid cancers such as invasive breast adenocarcinoma.[33] However, no experimental methods have been developed to clarify this phenomenon. We previously showed that GBM cells migrate along an aligned fibrous scaffold and that their migration velocity depends on the fiber density.[24] By applying this experimental system, we investigated cell migration at the single-cell level using a fibrous substrate. To our knowledge, this is the first report of U87-MG cells showing increased unidirectional migration compared with that of cell lines derived from other solid cancers.

Epithelial-mesenchymal transitions play important roles in invasion.[34] Mesenchymal cells are characterized by an elongated spindle shape and migration along the fibrous extracellular matrix structure.[35−37] GBM cells are malignant cancer cells with mesenchymal characteristics.[38,39] Our fiber-based assay is suitable for analyzing the migration of cells with mesenchymal properties and is ideal for quantifying single-cell directional movement.[40,41] The fabricated fibers were aligned and uniform in diameter, inexpensively produced, and ready for use in repeated experiments.

We also examined the cytoskeletal dynamics of cells during migration using a fluorescent dye.[29] As shown in the results, tubulin expression was observed locally at the front edge of migrating cells. It has been suggested that cell migration is induced by tubulin remodeling[42,43] and that microtubule formation is involved in the development of the leading edge of cells and directional migration.[44] Our observations, based on using single-fiber-based cultures, clearly support these previous findings; however, the mechanism describing how the microtubules reorganize, and what triggers this reorganization, should be clarified.

https://doi.org/10.1021/acsabm.2c00958
ACS Appl. Bio Mater. 2023, 6, 765−773

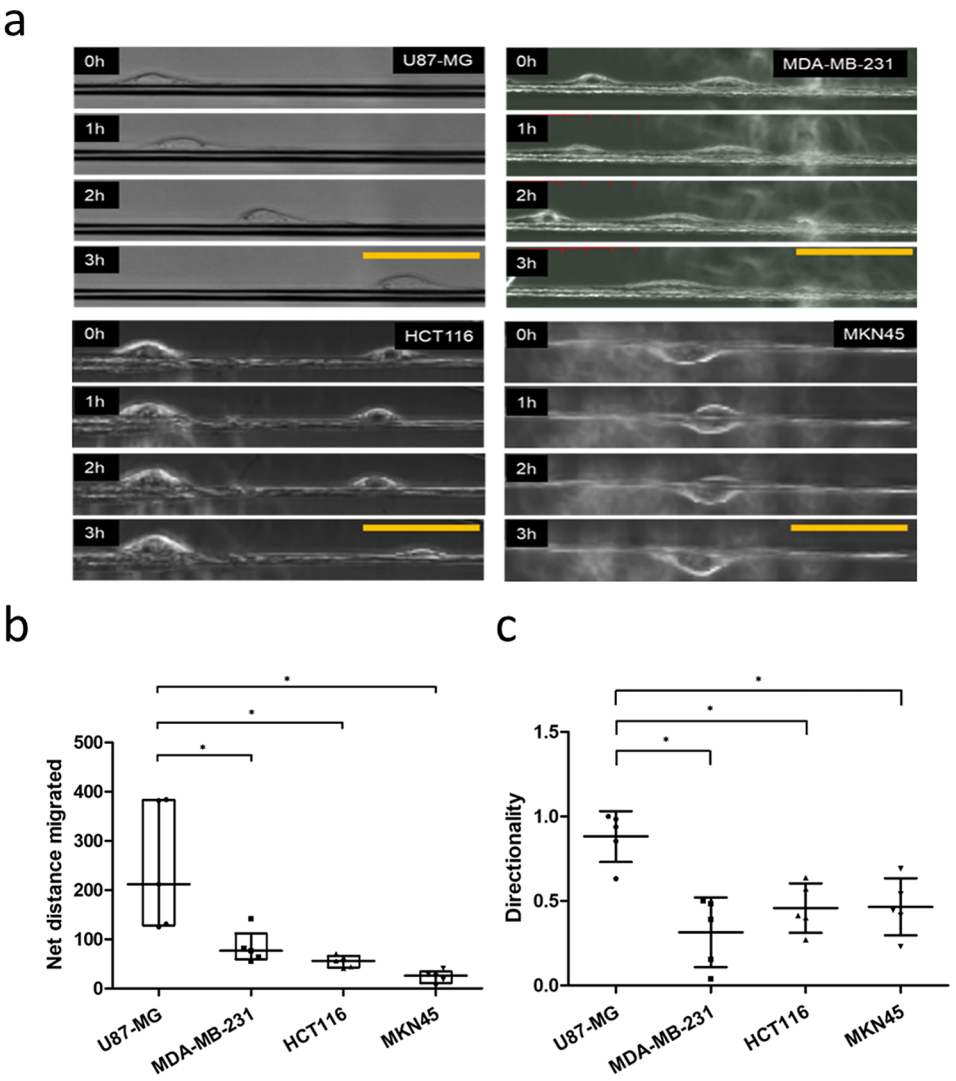

Figure 4. U87-MG cells showed the fastest migration by the fiber-based single-cell migration assay. (a) Representative cells migrating along a fiber at 0, 1, 2, and 3 h. Scale bar = 200 μm. (b) Migrated distance of cells cultured on a fiber scaffold for 3 h. Values represent medians and IQR. (c) Directionality of migration of each cell type along the fiber. Migration was assessed after 3 h. Values represent means ± SD n = 5; *p < 0.05.

Protein and mRNA expression in GBM cells is altered in cells elongated on fibrous structures.[45,46] Investigating fast-moving cells is one method for understanding gene expression in invading cells.[47] In this study, we used noncoated fibers, but the microenvironment of the extracellular matrix has a profound role in cellular migration. The fiber-based culture conditions we developed could be adapted to include coating the fiber surface with extracellular matrix proteins or cytokines. This might allow the development of experimental models that more closely mimic the specific brain microenvironment *in vivo*.[48−50] Moreover, the nanotopography of the nanofiber scaffold on cell migration could affect cell migration through mechanical stimuli. An aligned nanotopography has been demonstrated to alter the expression of cell differentiation[51] and migratory genes.[45] In this study, the influence of the tension of bridged nanofibers might affect cell behaviors such as migration. The GBM tumor microenvironment is known to be associated with hypoxia[52] and acidity.[53] Hence, mimicking these environments is also critical for accurately assessing the migration characteristics of GBM cells during tumor progression and metastasis. These should be considered in future studies.

Drugs targeting microtubules, such as microtubule inhibitors,[54] suppress tumor growth and migration.[55,56] To screen these drugs, analyses using immunolabeling are required; however, it has been difficult to correlate these analyses with dynamic and quantitative methods that investigate cell directionality and polarity. Our method described here is facile; it allows for the detection of the migration of invasive cells in simultaneous combination with conventional immunolabeling methods. This approach can be used to localize the expression of microtubules and related proteins, leading to a better understanding of the dynamism of cell invasion mechanisms. It would also facilitate the identification of candidate drugs targeting microtubules for the treatment of highly invasive cancers, but this investigation is still ongoing.

5. CONCLUSIONS

GBM cells exhibited the highest migratory ability, measured using a fiber model that mimics nerve fibers, among the four cancer cell lines in this study. The migratory ability in the fiber model was significantly higher than that in the conventional, wound healing, and transwell membrane assays. It would be possible to examine how changes in the microcellular

https://doi.org/10.1021/acsabm.2c00958
ACS Appl. Bio Mater. 2023, 6, 765−773

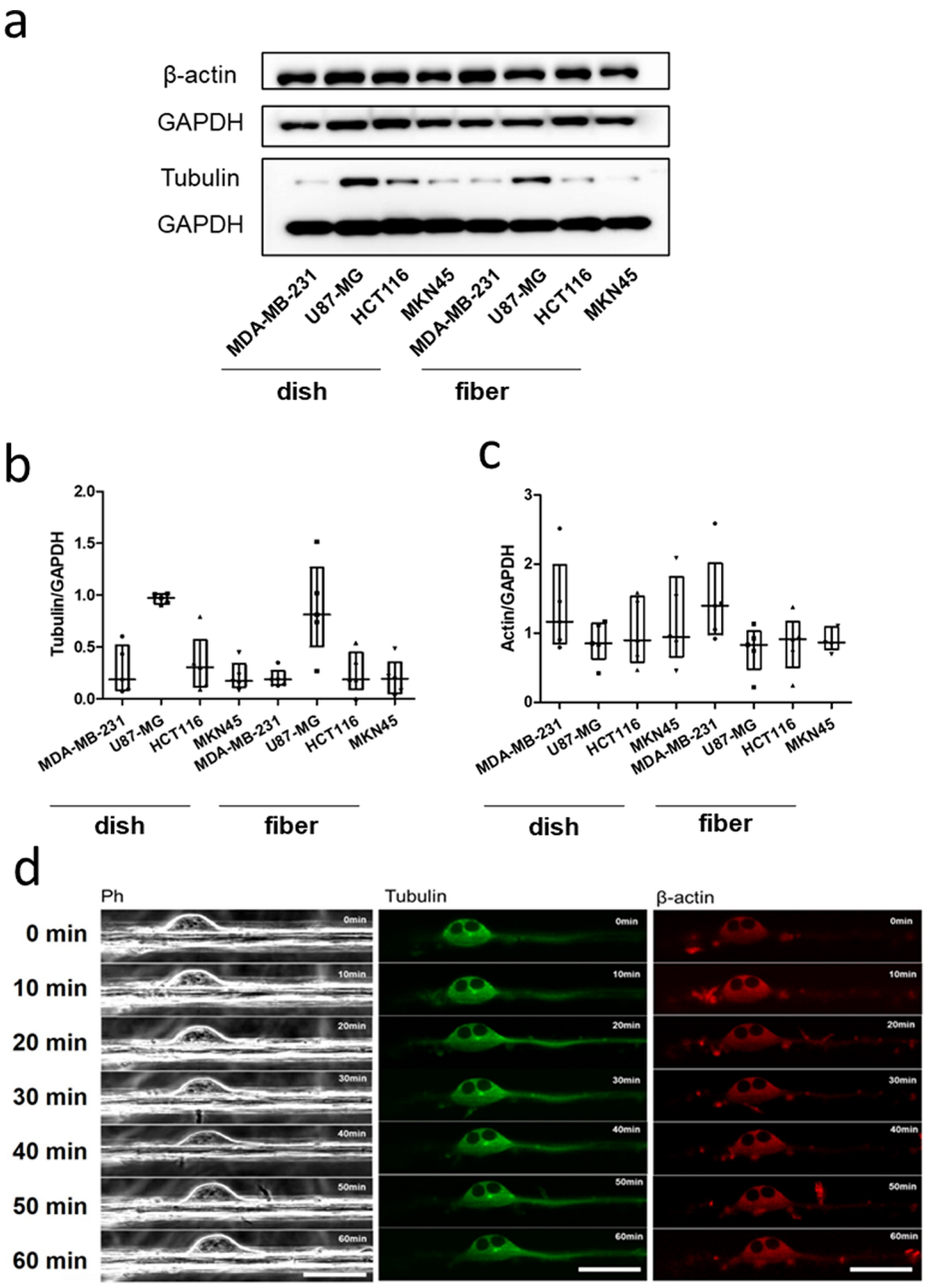

Figure 5. U87-MG cells showed a high expression level of tubulin, which was localized along the leading edge of an elongating cell. (a) Western blot. (b) Quantitative analysis of the tubulin/GAPDH ratio. (c) Quantitative analysis of the actin/GAPDH ratio. Values represent medians and IQR. n = 5. (d) Time-lapse microscopy of cytoskeletal localization in a U-87 MG cell cultured on a fiber from 0 to 60 min. Cells were transduced with GFP-tubulin (green) and RFP-actin (red). Scale bar = 50 μm.

environment, including extracellular matrix, hypoxia, pH, and nanotopography, affect migratory ability by studying GBM cell migration using the fiber model in the future. Our fiber-based assay would allow investigations of the mechanism of tumor cell migration and the discovery of migration inhibitors, leading to innovative approaches for GBM treatment.

■ ASSOCIATED CONTENT

Data Availability Statement

The data sets used and/or analyzed during the current study are available from the corresponding author on request.

Supporting Information

The Supporting Information is available free of charge at https://pubs.acs.org/doi/10.1021/acsabm.2c00958.

Figure S1. High-magnification SEM images of an electrospun fiber. **Figure S2.** Original gel images of the Western blot in Figure 5a. **Table S1.** Statistical analysis for Figure 5b. **Table S2.** Statistical analysis for Figure 5c (PDF)

Movie S1. Time-lapse microscopy of U-87 MG cells corresponding to Figure 4a (AVI)

Movie S2. Time-lapse microscopy of MDA-MB-213 cells corresponding to Figure 4a (AVI)

Movie S3. Time-lapse microscopy of HCT116 cells corresponding to Figure 4a (AVI)

https://doi.org/10.1021/acsabm.2c00958
ACS Appl. Bio Mater. 2023, 6, 765−773

Movie S4. Time-lapse microscopy of MKN45 cells corresponding to Figure 4a (AVI)

AUTHOR INFORMATION

Corresponding Authors

Norichika Hashimoto − *Division of Medicine, Department of Neurosurgery, Faculty of Medical Sciences, University of Fukui, Eiheiji-cho, Yoshida-gun, Fukui 910-1193, Japan; Department of Neurosurgery, Fukui General Hospital, Fukui-shi, Fukui 910-8561, Japan*; Email: hashi1972@eagle.ocn.ne.jp

Satoshi Fujita − *Department of Frontier Fiber Technology and Science, Graduate School of Engineering and Organization for Life Science Advancement Programs, University of Fukui, Fukui-shi, Fukui 910-8507, Japan*; orcid.org/0000-0003-1438-6402; Email: fujitas@u-fukui.ac.jp

Authors

Ryuhei Kitai − *Division of Medicine, Department of Neurosurgery, Faculty of Medical Sciences, University of Fukui, Eiheiji-cho, Yoshida-gun, Fukui 910-1193, Japan; Department of Neurosurgery, Kaga Medical Center, Kaga-shi, Ishikawa 922-8522, Japan*

Takahiro Yamauchi − *Division of Medicine, Department of Neurosurgery, Faculty of Medical Sciences, University of Fukui, Eiheiji-cho, Yoshida-gun, Fukui 910-1193, Japan; Organization for Life Science Advancement Programs, University of Fukui, Fukui-shi, Fukui 910-8507, Japan*

Makoto Isozaki − *Division of Medicine, Department of Neurosurgery, Faculty of Medical Sciences, University of Fukui, Eiheiji-cho, Yoshida-gun, Fukui 910-1193, Japan*

Ken-Ichiro Kikuta − *Division of Medicine, Department of Neurosurgery, Faculty of Medical Sciences, University of Fukui, Eiheiji-cho, Yoshida-gun, Fukui 910-1193, Japan; Organization for Life Science Advancement Programs, University of Fukui, Fukui-shi, Fukui 910-8507, Japan*

Complete contact information is available at: https://pubs.acs.org/10.1021/acsabm.2c00958

Author Contributions

N.H., S.F., and K.K. designed the study. N.H., T.Y., M.I., and S.F. performed the experiments and analyzed the data. N.H., R.K., S.F., and K.K. discussed the results and prepared the manuscript. All authors reviewed the manuscript.

Notes

The authors declare no competing financial interest.

ACKNOWLEDGMENTS

This work was supported by the Japan Society for the Promotion of Science (JSPS; Grants-in-Aid for Scientific Research, 19K09502, 21K09172) and the Life Science Innovation Center at the University of Fukui. The authors acknowledge Editage (www.editage.jp) for English proofing.

ABBREVIATIONS

GBM, Glioblastoma
DMEM, Dulbecco's modified Eagle's medium
FBS, Fetal bovine serum
IQR, Interquartile range
SEM, Scanning electron microscopy
PBS, Phosphate buffered saline
RIPA, Radioimmunoprecipitation
GAPDH, Glyceraldehyde-3-phosphate dehydrogenase

REFERENCES

(1) Perry, J. R.; Laperriere, N.; O'Callaghan, C. J.; Brandes, A. A.; Menten, J.; Phillips, C.; Fay, M.; Nishikawa, R.; Cairncross, J. G.; Roa, W.; Osoba, D.; Rossiter, J. P.; Sahgal, A.; Hirte, H.; Laigle-Donadey, F.; Franceschi, E.; Chinot, O.; Golfinopoulos, V.; Fariselli, L.; Wick, A.; Feuvret, L.; Back, M.; Tills, M.; Winch, C.; Baumert, B. G.; Wick, W.; Ding, K.; Mason, W. P. Short-course radiation plus Temozolomide in elderly patients with glioblastoma. *N Engl J. Med.* **2017**, *376* (11), 1027−1037.

(2) Stupp, R.; Mason, W. P.; van den Bent, M. J.; Weller, M.; Fisher, B.; Taphoorn, M. J. B.; Belanger, K.; Brandes, A. A.; Marosi, C.; Bogdahn, U.; Curschmann, J.; Janzer, C. R.; Ludwin, K. S.; Gorlia, T.; Allgeier, A.; Lacombe, D.; Cairncross, G. J.; Eisenhauer, E.; Mirimanoff, O. R. Radiotherapy plus concomitant and adjuvant Temozolomide for glioblastoma. *N Engl J. Med.* **2005**, *352* (10), 987−996.

(3) Mangiola, A.; de Bonis, P.; Maira, G.; Balducci, M.; Sica, G.; Lama, G.; Lauriola, L.; Anile, C. Invasive tumor cells and prognosis in a selected population of patients with glioblastoma multiforme. *Cancer* **2008**, *113* (4), 841−846.

(4) Xie, Q.; Mittal, S.; Berens, E. M. Targeting adaptive glioblastoma: an overview of proliferation and invasion. *Neuro Oncol* **2014**, *16* (12), 1575−1584.

(5) Ahir, K. B.; Engelhard, H. H.; Lakka, S. S. Tumor development and angiogenesis in adult brain tumor: Glioblastoma. *Mol. Neurobiol* **2020**, *57* (5), 2461−2478.

(6) Paw, I.; Carpenter, C. R.; Watabe, K.; Debinski, W.; Lo, W. H. Mechanisms regulating glioma invasion. *Cancer Lett.* **2015**, *362* (1), 1−7.

(7) Stummer, W.; Reulen, J. H.; Meinel, T.; Pichlmeier, U.; Schumacher, W.; Tonn, C. J.; Rohde, V.; Oppel, F.; Turowski, B.; Woiciechowsky, C.; Franz, K.; Pietsch, T.; ALA-Glioma Study Group. Extent of resection and survival in glioblastoma multiforme: identification of and adjustment for bias. *Neurosurgery* **2008**, *62* (3), 564−576.

(8) Giese, A.; Westphal, M. Glioma invasion in the central nervous system. *Neurosurgery* **1996**, *39* (2), 235−252.

(9) Lu, V. M.; Jue, T. R.; McDonald, K. L.; Rovin, R. A. The survival effect of repeat surgery at glioblastoma recurrence and its trend: A systematic review and meta-analysis. *World Neurosurgery* **2018**, *115*, 453−459.e3.

(10) Peiffer, J.; Kleihues, P. Hans-Joachim Scherer (1906−1945), pioneer in glioma research. *Brain Pathol* **1999**, *9* (2), 241−245.

(11) Scherer, H. J. A critical review: The pathology of cerebral gliomas. *J. Neurol Psychiatry* **1940**, *3* (2), 147−177.

(12) Zagzag, D.; Esencay, M.; Mendez, O.; Yee, H.; Smirnova, I.; Huang, Y.; Chiriboga, L.; Lukyanov, E.; Liu, M.; Newcomb, E. W. Hypoxia- and vascular endothelial growth factor-induced stromal cell-derived factor-1alpha/CXCR4 expression in glioblastomas: one plausible explanation of Scherer's structures. *Am. J. Pathol.* **2008**, *173* (2), 545−560.

(13) D'Alessio, A.; Proietti, G.; Sica, G.; Scicchitano, M. B. Pathological and molecular features of glioblastoma and its peritumoral tissue. *Cancer* **2019**, *11* (4), 469.

(14) Monzo, P.; Chong, K. Y.; Guetta-Terrier, C.; Krishnasamy, A.; Sathe, R. S.; Yim, F. K. E.; Ng, H. W.; Ang, T. B.; Tang, C.; Ladoux, B.; Gauthier, C. N.; Sheetz, P. M. Mechanical confinement triggers glioma liner migration dependent on forming FHOD3. *Mol. Biol. Cell* **2016**, *27* (8), 1246−1261.

(15) Velasquez, C.; Caballero, H.; Vazquez-Barquero, A.; Vega, M.; Rial, C. J.; Carcedo-Barrio, C. M.; Martino, J. Insular gliomas with exophytic extension to the Sylvian cistern: A glioma growth pattern that has gone previously unnoticed. *World Neurosurg* **2016**, *87*, 200−206.

(16) Zhang, Y.; Weinberg, A. R. Epithelial-to-mesenchymal transition in cancer: complexity and opportunities. *Front Med.* **2018**, *12* (4), 361−373.

(17) Benseddik, K.; Sen Nkwe, S.; Daou, P.; Verdier-Pinard, P.; Badache, A. ErbB2-dependent chemotaxis requires microtubule capture and stabilization coordinated by distinct signaling pathways. *PLoS One* **2013**, *8* (1), No. e55211.
(18) Wakuda, Y.; Nishimoto, S.; Suye, S.; Fujita, S. Native collagen hydrogel nanofibers with anisotropic structure using core-shell electrospinning. *Sci. Rep* **2018**, *8* (1), 6248.
(19) Lee, J.; Ryu, Y.; Ji, Y.; Kang, Y. J.; Moon, E. Hypoxia/reoxygenation-experienced cancer cell migration and metastasis are regulated by Rap1- and Rac1-GTPase activation via the expression of thymosin beta-4. *Oncotarget* **2015**, *6* (12), 9820−9833.
(20) Grada, A.; Otero-Vinas, M.; Prieto-Castrillo, F.; Obagi, Z.; Falanga, V. Research techniques made simple: Analysis of collective cell migration using the wound healing assay. *J. Invest Dermal* **2017**, *137* (2), e11−e16.
(21) Oh, J.-M.; Venters, C. C.; Di, C.; Pinto, M. A.; Wan, L.; Younis, I.; Cai, Z.; Arai, C.; So, R. B.; Duan, J.; Dreyfuss, G. U1 snRNP regulates cancer cell migration and invasion in vitro. *Nat. Commun.* **2020**, *11* (1), 1.
(22) Lintz, M.; Muñoz, A.; Reinhart-King, C. A. The mechanics of single cell and collective migration of tumor cells. *J. Biomech Eng.* **2017**, *139* (2), 021005.
(23) Beadle, C.; Assanah, M. C.; Monzo, P.; Vallee, R.; Rosenfeld, S. S.; Canoll, P. The role of myosin II in glioma invasion of the brain. *Mol. Biol. Cell* **2008**, *19* (8), 3357−3368.
(24) Huang, W. Y.; Suye, S. I.; Fujita, S. Cell trapping via migratory inhibition within density-tuned electrospun nanofibers. *ACS Appl. Bio Mater.* **2021**, *4* (10), 7456−7466.
(25) Fan, M.; Arai, M.; Tawada, A.; Chiba, T.; Fukushima, R.; Uzawa, K.; Shiiba, M.; Kato, N.; Tanzawa, H.; Takiguchi, Y. Contrasting functions of the epithelial-stromal interaction 1 gene, in human oral and lung squamous cell cancers. *Oncol. Rep.* **2021**, *47* (1), 5.
(26) Bauer, M.; Nascakova, Z.; Mihai, A. I.; Cheng, P. F.; Levesque, M. P.; Lampart, S.; Hurwitz, R.; Pfannkuch, L.; Dobrovolna, J.; Jacobs, M.; Bartfeld, S.; Dohlman, A.; Shen, X.; Gall, A. A.; Salama, N. R.; Töpfer, A.; Weber, A.; Meyer, T. F.; Janscak, P.; Müller, A. The ALPK1/TIFA/NF-κB axis links a bacterial carcinogen to R-loop-induced replication stress. *Nat. Commun.* **2020**, *11* (1), 5117.
(27) Kang, Y. J.; Bang, B. R.; Han, K. H.; Hong, L.; Shim, E. J.; Ma, J.; Lerner, R. A.; Otsuka, M. Regulation of NKT cell-mediated immune responses to tumours and liver inflammation by mitochondrial PGAM5-Drp1 signalling. *Nat. Commun.* **2015**, *6*, 8371.
(28) Rol, Á; Todorovski, T.; Martin-Malpartida, P.; Escolà, A.; Gonzalez-Rey, E.; Aragón, E.; Verdaguer, X.; Vallès-Miret, M.; Farrera-Sinfreu, J.; Puig, E.; Fernández-Carneado, J.; Ponsati, B.; Delgado, M.; Riera, A.; Macias, M. J. Structure-based design of a Cortistatin analogue with immunomodulatory activity in models of inflammatory bowel disease. *Nat. Commun.* **2021**, *12* (1), 1869.
(29) Ames, S. R.; Kost, A. T.; Condreay, J. P. BacMam technology and its application to drug discovery. *Expert Opin Drug Discov* **2007**, *2* (12), 1669−1681.
(30) Lah, T. T.; Novak, M.; Breznik, B. Brain malignancies: Glioblastoma and brain metastases. *Semin Cancer Biol.* **2020**, *60*, 262−273.
(31) Kitai, R.; Horita, R.; Sato, K.; Yoshida, K.; Arishima, H.; Higashino, Y.; Hashimoto, N.; Takeuchi, H.; Kubota, T.; Kikuta, K. Nestin expression in astrocytic tumors delineates tumor infiltration. *Brain Tumor Pathol* **2010**, *27* (1), 17−21.
(32) Giese, A.; Kluwe, L.; Laube, B.; Meissner, H.; Berens, E. M.; Westphal, M. Migration of human glioma cells on myelin. *Neurosurgery* **1996**, *38* (4), 755−764.
(33) Nelson, T. M.; Short, A.; Cole, L. S.; Gross, C. A.; Winter, J.; Eubank, D. T.; Lannutti, J. J. Preferential, enhanced breast cancer cell migration on biomimetic electrospun nanofiber 'cell highways'. *BMC Cancer* **2014**, *14*, 825.
(34) Vollmann-Zwerenz, A.; Leidgens, V.; Feliciello, G.; Klein, A. C.; Hau, P. Tumor cell invasion in glioblastoma. *Int. J. Mol. Sci.* **2020**, *21* (6), 1932.
(35) Enam, A. S.; Rosenblum, L. M.; Edvardsen, K. Role of extracellular matrix in tumor invasion: migration of glioma cells along fibronectin-positive mesenchymal cell processes. *Neurosurgery* **1998**, *42* (3), 599−608.
(36) Sharma, P.; Sheets, K.; Elankumaran, S.; Nain, S. A. The mechanistic influence of aligned nanofibers on cell shape, migration and blebbing dynamics of glioma cells. *Integr Bio* **2013**, *5* (8), 1036−1044.
(37) Guetta-Terrier, C.; Monzo, P.; Zhu, J.; Long, H.; Venkatraman, L.; Zhou, Y.; Wang, P.; Chew, Y. S.; Mogilner, A.; Ladoux, B.; Gauthier, N. C. Protrusive waves guide 3D cell migration along nanofibers. *J. Cell Biol.* **2015**, *211* (3), 683−701.
(38) Meel, H. M.; Schaper, A. S.; Kaspers, JL G; Hulleman, E. Signaling pathways and mesenchymal transition in pediatric high-grade glioma. *Cell. Mol. Life Sci.* **2018**, *75* (5), 871−887.
(39) Majc, B.; Sever, T.; Zarić, M.; Breznik, B.; Turk, B.; Lah, T. T. Epithelial-to-mesenchymal transition as the driver of changing carcinoma and glioblastoma microenvironment. *Biochim Biophys Acta Mol. Cell Res.* **2020**, *1867* (10), 118782.
(40) Johnson, J.; Nowicki, O. M.; Lee, H. C.; Chiocca, E. A.; Viapiano, S. M.; Lawler, S. E.; Lannutti, J. J. Quantitative analysis of complex glioma cell migration on electrospun polycaprolactone using time-lapse microscopy. *Tissue Eng. Part C Methods.* **2009**, *15* (4), 531−540.
(41) Rao, S. S.; Nelson, T. M.; Xue, R.; DeJesus, K. J.; Viapiano, S. M.; Lannutti, J. J.; Sarkar, A.; Winter, J. O. Mimicking white matter tract topography using coreshell electrospun nanofibers to examine migration of malignant brain tumors. *Biomaterials* **2013**, *34* (21), 5181−5190.
(42) Garcin, C.; Straube, A. Microtubules in cell migration. *Essays Biochem* **2019**, *63* (5), 509−520.
(43) Seetharaman, S.; Etienne-Manneville, S. Cytoskeletal crosstalk in cell migration. *Trends Cell Biol.* **2020**, *30* (9), 720−735.
(44) Mimori-Kiyosue, Y. Shaping microtubules into diverse patterns: Molecular connections for setting up both ends. *Cytoskeleton* **2011**, *68*, 603−618.
(45) Beliveau, A.; Thomas, G.; Gong, J.; Wen, Q.; Jain, A. Aligned nanotopography promotes a migratory state in glioblastoma multiforme tumor cells. *Sci. Rep* **2016**, *6*, 26143.
(46) Agudelo-Garcia, A. P.; De Jesus, J. K.; Williams, P. S.; Nowicki, O. M.; Chiocca, A. E.; Liyanarachchi, S.; Li, P.-K.; Lannutti, J. J.; Johnson, K. J.; Lawler, E. S.; Viapiano, S. M. Glioma cell migration on three-dimensional nanofiber scaffolds is regulated by substrate topography and abolished by inhibition of STAT3 signaling. *Neoplasia* **2011**, *13* (9), 831.
(47) Schönholzer, M. T.; Migliavacca, J.; Alvarez, E.; Santhana Kumar, K.; Neve, A.; Gries, A.; Ma, M.; Grotzer, M. A.; Baumgartner, M. Real-time sensing of MAPK signaling in medulloblastoma cells reveals cellular evasion mechanism counteracting dasatinib blockade of ERK activation during invasion. *Neoplasia* **2020**, *22* (10), 470−483.
(48) Yamada, M. K.; Sixt, M. Mechanisms of 3D cell migration. *Nat. Rev. Mol. Cell Biol.* **2019**, *20* (12), 738−752.
(49) Doyle, D. A.; Wang, W. F.; Matsumoto, K.; Yamada, M. K. One-dimensional topography underlies three-dimensional fibrillar cell migration. *J. Cell Biol.* **2009**, *184* (4), 481−490.
(50) Estabridis, M. H.; Jana, A.; Nain, A.; Odde, J. D. Cell migration in 1D and 2D nanofiber microenvironments. *Ann. Biomed Eng.* **2018**, *46* (3), 392−403.
(51) Fujita, S.; Shimizu, H.; Suye, S. Control of differentiation of human mesenchymal stem cells by altering the geometry of nanofibers. *J. Nanotechnol* **2012**, *2012*, 429890.
(52) Wang, G.; Wang, J. J.; Fu, X. L.; Guang, R.; To, S. T. Advances in the targeting of HIF-1alfa and future therapeutic strategies for glioblastoma multiforme. *Oncol. Rep.* **2017**, *37*, 657−670.
(53) Webb, B. A.; Chimenti, M.; Jacobson, M. P.; Barber, D. L. Dysregulated pH: a perfect storm for cancer progression. *Nat. Rev. Cancer* **2011**, *11* (9), 671.
(54) Eitaki, M.; Yamamori, T.; Meike, S.; Yasui, H.; Inanami, O. Vincristine enhances amoeboid-like motility via GEF-H1/RhoA/

https://doi.org/10.1021/acsabm.2c00958
ACS Appl. Bio Mater. 2023, 6, 765−773

ROCK/Myosin light chain signaling in MKN45 cells. *BMC Cancer* **2012**, *12*, 469.
(55) Cortes, J.; Schöffski, P.; Littlefield, A. B. Multiple modes of action of eribulin mesylate: Emerging data and clinical implications. *Cancer Treat Rev.* **2018**, *70*, 190−198.
(56) Ranganath, H. S.; Fu, Y.; Arifin, Y. D.; Kee, I.; Zheng, L.; Lee, H. S.; Chow, K-H P; Wang, C.-H. The use of submicron/nanoscale PLGA implants to deliver paclitaxel with enhanced pharmacokinetics and therapeutic efficacy in intracranial glioblastoma in mice. *Biomaterials* **2010**, *31* (19), 5199−5207.

https://doi.org/10.1021/acsabm.2c00958
ACS Appl. Bio Mater. 2023, 6, 765−773